IDENTIFICATION AND MODELING OF AMB ROTOR SYSTEM USING COMPLEX LEAD AND LAG COMPENSATOR STRUCTURES

Katja Hynynen, Rafal Jastrzebski, Riku Pöllänen

Dep. of Electrical Eng., Lappeenranta University of Technology, 53851 Lappeenranta, Finland

katja.hynynen@lut.fi

ABSTRACT

Control design of AMB rotor system demands very accurate system model. Modeling of the rotor is traditionally made using Finite Element Method (FEM) or Experimental Modal Analysis (EMA), but Active Magnetic Bearings (AMB) offer a possibility to obtain the model using system identification. The purpose of this study is to identify the flexible modes of the rotor and determine its transfer function model using complex lead and lag compensator structures. The results demonstrate that the proposed method suits for modeling the flexible modes of an AMB rotor system.

INTRODUCTION

The control of active magnetic bearing requires very accurate system model to operate reliably. Earlier it was widely thought that only the rigid modes would be sufficient to model the rotor. Nowadays the tendency in the industry applications is to reach higher integration and lower power consumption, which leads to rotors with flexible eigenmodes within the control system bandwidth. The modeling and control of these elastic modes take remarkable part of time, and hence cost, needed in AMB system design. [1] Traditionally the flexible eigenmodes of rotor are modeled either by mechanical hammer excitation or by FEM [2]. The mentioned methods are still in use but their results can be verified by system identification. This is done using the AMB with the rotor already installed and with existing AMB controller program. [1], [3] System identification is also suitable for fault diagnostics during operation.

Since the parametric methods do not give correct poles for AMB system, nonparametric identification methods are used. The obtained nonparametric Frequency Response Function (FRF) is converted to parametric model, that is a transfer function model, using complex lead and lag compensator structures [4]. Major advance of the proposed method is a graphical presentation that makes it very illustrative and simple to use.

MODELING OF AMB ROTOR SYSTEM

Flexible modes of the rotor are typically modeled using modal coordinates. The equation of motion of an AMB rotor system with a constant rotation speed Ω in modal coordinates is

$$\mathbf{M}\ddot{\boldsymbol{\eta}} + (\mathbf{D} + \Omega\mathbf{G})\dot{\boldsymbol{\eta}} + \mathbf{K}\boldsymbol{\eta} = \boldsymbol{\Psi}^T\mathbf{f}$$
$$\mathbf{z} = \boldsymbol{\Phi}\boldsymbol{\eta} \qquad (1)$$

where $\mathbf{M}$, $\mathbf{D}$ and $\mathbf{K}$ are diagonal mass, damping and stiffness matrices and $\mathbf{G}$ is a gyroscopic matrix of the rotor in modal coordinates. $\boldsymbol{\eta}$ is modal displacement vector, $\mathbf{f}$ is force input and $\mathbf{z}$ sensor output. Matrices $\boldsymbol{\Phi}$ and $\boldsymbol{\Psi}$ are composed of the vectors $\varphi_{r,f}$ and $\psi_{r,f}$ that describe the displacements of eigenforms of the rotor from the sensor and actuator

$$\boldsymbol{\Phi} = \begin{bmatrix} | & | & | & | & | \\ \varphi_{r=1} & \varphi_{r=2} & \varphi_{f=1} & \cdots & \varphi_{f=n} \\ | & | & | & | & | \end{bmatrix}, \qquad (2)$$

$$\boldsymbol{\Psi} = \begin{bmatrix} | & | & | & | & | \\ \psi_{r=1} & \psi_{r=2} & \psi_{f=1} & \cdots & \psi_{f=n} \\ | & | & | & | & | \end{bmatrix}. \qquad (3)$$

Subscripts r and f refer to rigid and flexible modes. When considering a non-rotating rotor ($\Omega = 0$), there are no gyroscopic effects and Eq. (1) simplifies to

$$\mathbf{M}\ddot{\boldsymbol{\eta}} + \mathbf{D}\dot{\boldsymbol{\eta}} + \mathbf{K}\boldsymbol{\eta} = \boldsymbol{\Psi}^T\mathbf{f}$$
$$\mathbf{z} = \boldsymbol{\Phi}\boldsymbol{\eta} \qquad (4)$$

State equation of the AMB system is

$$\dot{\mathbf{x}} = \mathbf{A}\mathbf{x} + \mathbf{B}\mathbf{u}$$
$$\mathbf{y} = \mathbf{C}\mathbf{x} \qquad (5)$$

where the state matrices are

$$\mathbf{A} = \begin{bmatrix} \mathbf{0} & \mathbf{I} \\ -\mathbf{M}^{-1}\mathbf{K} & -\mathbf{M}^{-1}\mathbf{D} \end{bmatrix}, \tag{6}$$

$$\mathbf{B} = \begin{bmatrix} \mathbf{0} \\ \mathbf{\Psi}^T \end{bmatrix}, \tag{7}$$

$$\mathbf{C} = \begin{bmatrix} \mathbf{\Phi} & \mathbf{0} \end{bmatrix}. \tag{8}$$

State equation (5) can be converted to transfer function matrix with equation

$$\mathbf{h}(s) = \mathbf{C}(s\mathbf{I} - \mathbf{A})^{-1}\mathbf{B}. \tag{9}$$

Substitute the state matrices (6)-(8) to Eq. (9) to get the transfer function matrix of AMB rotor system

$$\mathbf{h}(s) = \mathbf{\Phi}(s^2 + \mathbf{M}^{-1}\mathbf{D}s + \mathbf{M}^{-1}\mathbf{K})^{-1}\mathbf{\Psi}^T. \tag{10}$$

Mass-normalized coordinates are used, and hence mass is a unity vector $\mathbf{M} = \mathbf{I}$. Damping and stiffness matrices are

$$\mathbf{K} = \mathrm{diag}\left(\begin{bmatrix} -p_1^2 & -p_2^2 & \omega_{p1}^2 & \ldots & \omega_{pn}^2 \end{bmatrix}\right), \tag{11}$$

$$\mathbf{D} = 2\mathrm{diag}\left(\begin{bmatrix} d_1 & d_2 & \zeta_1\omega_{p1} & \ldots & \zeta_n\omega_{pn} \end{bmatrix}\right), \tag{12}$$

where $p_{1,2}$ are poles and $d_{1,2}$ dampings of the rigid body modes. $\omega_{p1} \ldots \omega_{pn}$ are natural frequencies of flexible mode poles and $\zeta_{1,...,n}$ are damping ratios of the flexible modes. Substitution of Eq. (11)-(12) into Eq. (10) gives

$$\mathbf{h}(s) = \sum_{r=1}^{2} \frac{\mathbf{R}_r}{s^2 + 2d_r s - p_r^2} + \sum_{f=1}^{n} \frac{\mathbf{R}_f}{s^2 + 2\zeta_f\omega_{pf}s + \omega_{pf}^2}, \tag{13}$$

where residual terms $\mathbf{R}_r$ and $\mathbf{R}_f$ are dyadic products [1], [5]

$$\begin{aligned} \mathbf{R}_r &= \varphi_r\psi_r^T, \\ \mathbf{R}_f &= \varphi_f\psi_f^T. \end{aligned} \tag{14}$$

Eq. (13) is a parallel mode representation of the AMB rotor system. The same can be represented in serial mode, which is used further in the paper when converting the system FRF to a transfer function model.

IDENTIFICATION
AMB rotor system is a multiple input, multiple output (MIMO) system with four inputs and four outputs. In order to distinguish the influence of each input on each output, at least as many distinct measurements must be made as there are system outputs. In this paper the system is considered to consist of several single input,

multiple output (SIMO) systems, for which the traditional identification methods are valid.

Nonparametric methods
Simplest nonparametric identification method of FRF is Empirical Transfer Function Estimate (ETFE)

$$\hat{G}_N(e^{i\omega}) = \frac{Y_N(\omega)}{U_N(\omega)}, \tag{15}$$

where $Y_N(\omega)$ and $U_N(\omega)$ are Discrete Fourier Transforms (DFT) of output and input, respectively,

$$Y_N(\omega) = \frac{1}{\sqrt{N}}\sum_{t=1}^{N} y(t)e^{-i\omega t}, \tag{16}$$

$$U_N(\omega) = \frac{1}{\sqrt{N}}\sum_{t=1}^{N} u(t)e^{-i\omega t} \tag{17}$$

and $\omega = 2\pi k/N, \quad k = 0,1,\ldots,N-1$.

ETFE gives a good performance for periodic input signals, especially for those frequencies that are present in input. However, when the input signal is aperiodic, which is the case in most systems with disturbances, the ETFE gives only a very rough estimate.

Systems with disturbances are better dealt with spectral analysis method where ETFE is smoothed using weighting functions. There it is assumed that the values of the true transfer function at different frequencies are related. The smoothed ETFE can be written as

$$\hat{G}_N(e^{i\omega_0}) = \frac{\int_{-\pi}^{\pi} W_\gamma(\xi - \omega_0)|U_N(\xi)|^2 \hat{G}_N(e^{i\xi})d\xi}{\int_{-\pi}^{\pi} W_\gamma(\xi - \omega_0)|U_N(\xi)|^2 d\xi}, \tag{18}$$

where $W_\gamma(\xi)$ is a weighting function or frequency window centered around the frequency $\xi = 0$. [6]

Transfer function of identified system
The frequency response obtained from identification is converted to transfer function for further use in controller design. For rigid modes, the a priori known model is used. For flexible modes the parametrized model is determined using complex lead and lag compensator method, where the suitable compensator structures are used for system modeling by matching their magnitude and phase shapes to the frequency response of the system [4].

The resonance peaks of the flexible modes of AMB system cause narrow peaks and notches in phase curve. These shapes can be modeled with complex lead and lag compensators, for which the general transfer function can be written

$$C_{\text{complex}}(s) = \frac{\omega_{\text{p}}}{\omega_{\text{z}}} \frac{s^2 + 2\zeta\omega_{\text{z}}s + \omega_{\text{z}}^2}{s^2 + 2\zeta\omega_{\text{p}}s + \omega_{\text{p}}^2}. \qquad (19)$$

The poles and zeros of such a compensator are complex conjugates with same damping ratio ζ, which leads to a symmetric phase lead or lag.

Further only the lead compensator is considered, but the same holds for lag compensator.

Eq. (19) represents a flexible mode component for a serial mode transfer function of AMR rotor system that can be used instead of the parallel mode transfer function of Eq. (13).

One possibility to match the compensator transfer function into frequency response function shape, is to consider the width of the phase peak at half of the maximum phase lead. Figure 1 shows the Bode plot of complex lead compensator and some features related to the mentioned method.

At first the phase lead of the compensator is determined. For a conventional lead compensator, the phase lead is ϕ_{m}, but for the complex one it is $2\phi_{\text{m}}$. Further the frequencies $\omega_{50\%}^+$ and $\omega_{50\%}^-$ at which the phase is one half of its maximum are determined. The frequency of maximum phase lead ω_{m} is in geometric mean of the half phase peak frequencies

$$\omega_{\text{m}} = \sqrt{\omega_{50\%}^+ \omega_{50\%}^-} \qquad (20)$$

and the estimated damping ratio is

$$\zeta \approx \frac{\omega_{50\%}^+ - \omega_{50\%}^-}{2\omega_{\text{m}}}. \qquad (21)$$

Now the compensator pole and zero are calculated from [4]

$$\omega_{\text{p}} = \omega_{\text{m}}\left(\zeta \tan\phi_{\text{m}} + \sqrt{\zeta^2 \tan^2\phi_{\text{m}} + 1} \right), \qquad (22)$$

$$\omega_{\text{z}} = \omega_{\text{m}}\left(-\zeta \tan\phi_{\text{m}} + \sqrt{\zeta^2 \tan^2\phi_{\text{m}} + 1} \right). \qquad (23)$$

Model validation

The validation of the obtained transfer function model is made by comparing its frequency response to the measured FRF and also to the FEM based model.

Additionally, the validity of the transfer function model is verified applying it to the frequency response curve of the known FEM based model and comparing the frequency responses and transfer functions of those two.
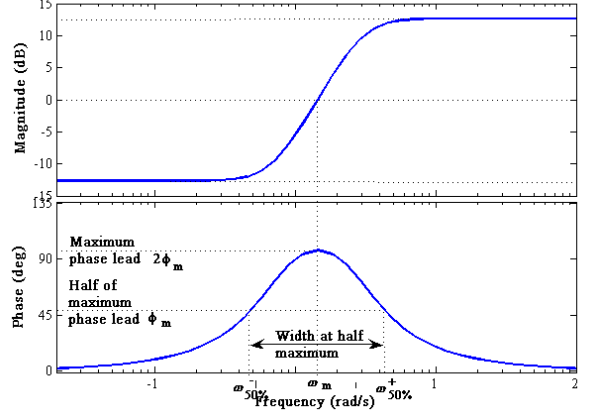

FIGURE 1: Some features of Bode plot of complex lead compensator.

Closed-loop measurement

As mentioned above, the AMB system is inherently unstable, and the use of a feedback controller is essential when running the system. However, the identification methods are meant for open-loop transfer function, so the open-loop model have to be determined from the closed-loop model. A block diagram of the system G_0 with feedback loop, disturbances and reference r are shown in Figure 2.

Now there are three possibilities to determine the open-loop transfer function G_0. The first is a direct approach where system input u and output y are used as in open-loop operation ignoring the feedback and the reference signal r. This is the best method, and its only drawback is that the disturbances must be well known. The second method is an indirect approach where the open-loop transfer function is determined from the closed-loop transfer function. In this method the controller must be known and it cannot contain nonlinearities. The third method is so called joint input-output identification that includes models for both input u and output y. The system input is

$$u(t) = r(t) + w(t) - F_{\text{y}}(q)y(t), \qquad (24)$$

where a non-measured disturbance in the controller $w(t)$ is independent of reference $r(t)$ and the measured disturbance $v(t)$. Now input and output are [6]

$$y = \frac{G_0}{1 + F_{\text{y}}G_0}r + \frac{1}{1 + F_{\text{y}}G_0}v + \frac{G_0}{1 + F_{\text{y}}G_0}w, \qquad (25)$$

$$u = \frac{1}{1 + F_{\text{y}}G_0}r - \frac{F_y}{1 + F_{\text{y}}G_0}v + \frac{1}{1 + F_{\text{y}}G_0}w. \qquad (26)$$
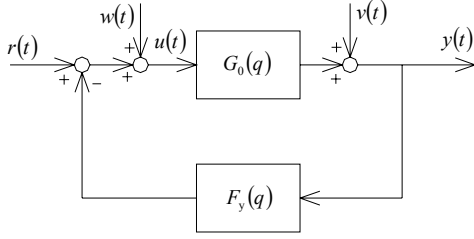
FIGURE 2: Block diagram of closed-loop system with disturbances $v(t)$ and $w(t)$ and the reference signal $r(t)$.

If all the system and sensor noises are assumed negligible, the AMB system transfer function can be written as

$$\frac{y}{u} = \frac{G_0(1 + F_y G_0)^{-1} r}{(1 + F_y G_0)^{-1} r} = G_0, \tag{27}$$

which means that the open-loop transfer function of AMB system can be obtained from the closed-loop measurements using direct method. [1]

RESULTS
The flexible modes of AMB system for non-rotating rotor are determined by identification. There is no gyroscopic effect and thus no coupling between radial planes. Therefore is sufficient to consider only one plane of the system.

Figure 3 shows the sketch of the rotor and the locations of the radial bearings A and B denoted by red stars. The green stars indicate the locations of the displacement sensors. The system also consists an axial bearing that is shown in the left end of the rotor. Also the mode shapes of the first three flexible modes determined by FEM, are presented in Figure 3.

Measurements
The A and B bearings are excited separately to avoid mixing of the excitation signals through the feedback branch. The excitation signal used in measurements is a sine sweep signal with an amplitude of 2 % of the maximum current. The frequency range of sweep signals is from 100 Hz to 1100 Hz. The radial rotor displacements and control currents are measured in both bearings A and B.

In identification process, the actuator of the AMB rotor system is supposed to be known. Also the rotor mass, and the distances of the bearings and sensors from mass center, are known. Due to the highly unstable nature of AMB system, it is impossible to run it without feedback controller, and hence a simple lead compensator with an integrator, designed according to rigid rotor dynamics is used. Rigid rotor transfer function matrix based on FEM is
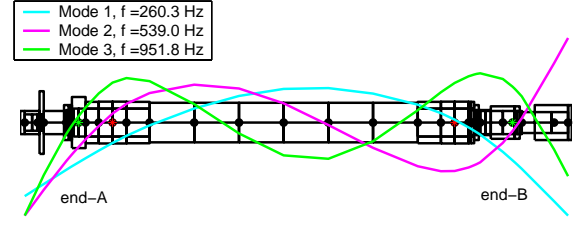
FIGURE 3: Rotor model with the mode shapes of the first three flexible modes. [7]

$$\mathbf{h}_r = \begin{bmatrix} h_{r11} & h_{r12} \\ h_{r21} & h_{r22} \end{bmatrix}, \tag{28}$$

where

$$h_{r11} = \frac{15.8(s^2 - 214^2)}{(s^2 - 239^2)(s^2 - 206^2)}, \tag{29}$$

$$h_{r12} = \frac{-4.5(s^2 - 156^2)}{(s^2 - 239^2)(s^2 - 206^2)}, \tag{30}$$

$$h_{r21} = \frac{-3.3(s^2 - 141^2)}{(s^2 - 239^2)(s^2 - 206^2)}, \tag{31}$$

$$h_{r22} = \frac{15.2(s^2 - 225^2)}{(s^2 - 239^2)(s^2 - 206^2)}, \tag{32}$$

Identification results
The frequency responses of the plant from control currents i_{cyA} and i_{cyB} to displacements y_A and y_B are shown in Figure 4. Solid blue line is the measured FRF, dashed red line is the frequency response of the transfer function model obtained using the fitted complex lead and lag compensators (TF model) and bold and solid green line is the frequency response formed according to the results obtained with FEM.
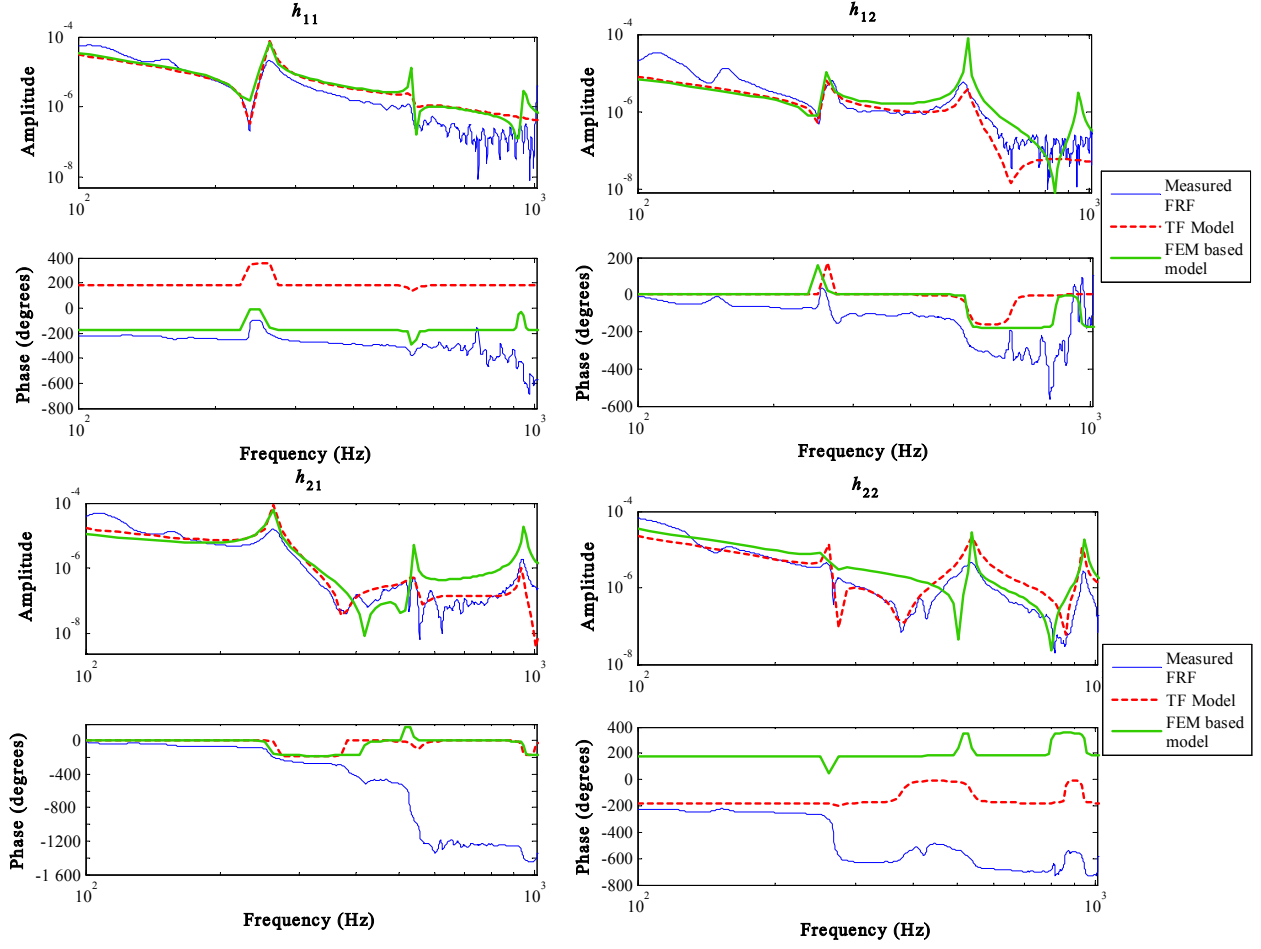
The FRF of the measured data is obtained using smoothed ETFE with Hamming window. The obtained transfer function matrix for first three (h_{11} and h_{12} only first two) flexible modes is

$$\mathbf{h}_f = \begin{bmatrix} h_{11} & h_{12} \\ h_{21} & h_{22} \end{bmatrix}, \tag{33}$$

where

$$h_{11} = \frac{(s^2 + 2s + 2.2 \cdot 10^6)(s^2 + 114s + 1.13 \cdot 10^7)}{(s^2 + 2s + 2.7 \cdot 10^6)(s^2 + 114s + 1.12 \cdot 10^7)}, \tag{34}$$

$$h_{12} = \frac{(s^2 + 2s + 2.6 \cdot 10^6)(s^2 + 143s + 1.8 \cdot 10^7)}{(s^2 + 2s + 2.7 \cdot 10^6)(s^2 + 114s + 1.1 \cdot 10^7)}, \tag{35}$$

FIGURE 4: Identification results. Frequency response functions of AMB rotor system from control currents i_{cAx} and i_{cBx} to rotor displacements x_A and x_B. Solid blue line is the measured FRF, dashed red line is the frequency response of the transfer function model and bold and solid green line of the FEM based model.

$$h_{21} = \frac{\left(s^2 + 3s + 5.5 \cdot 10^6\right)\left(s^2 + 120s + 1.2 \cdot 10^7\right)\left(s^2 + 77s + 4.1 \cdot 10^7\right)}{\left(s^2 + 2s + 2.7 \cdot 10^6\right)\left(s^2 + 114s + 1.1 \cdot 10^7\right)\left(s^2 + 71s + 3.5 \cdot 10^7\right)}, \quad (36)$$

$$h_{22} = \frac{\left(s^2 + 2s + 3.0 \cdot 10^6\right)\left(s^2 + 80s + 5.5 \cdot 10^6\right)\left(s^2 + 61s + 2.6 \cdot 10^7\right)}{\left(s^2 + 2s + 2.7 \cdot 10^6\right)\left(s^2 + 114s + 1.1 \cdot 10^7\right)\left(s^2 + 71s + 3.5 \cdot 10^7\right)} \quad (37)$$

Figure 4 shows that the identified transfer function model agrees quite well with the measured FRF with respect to the flexible modes. When comparing to the FEM based model, the poles are equivalent but the zeros differ, which is seen from Figure 4 and the transfer functions (34)-(37) and (33).

Some eigenmodes, for example the second mode in h_{11} and h_{21}, and the third mode in h_{11} and h_{12}, do not excite very well, which can be seen from Figure 4. The reason for this is shown in Figure 3.

According to Figure 3 the second eigenmode passes through the bearing A which affects to poor excitement of the mode in h_{11} and h_{21}. Similarly, the third eigenmode has a node at the sensor A and therefore the mode is not observable from sensor A measurement.

That is why the third mode is hardly noticeable in h_{11} and h_{12}. These will not cause problems in control because the modes can be filtered out.

The bad quality of the identified FRF in some frequencies makes the determination of the flexible modes in these frequencies difficult.

To verify the validity of the proposed method, it has been applied directly to the frequency response curve obtained with the known FEM based model. Figure 5 shows the FRFs for the FEM based model and for the transfer function model reconstructed from the previous one.

The corresponding transfer functions are

$$h_{F11} = \frac{\left(s^2 + 14s + 2.8 \cdot 10^6\right)\left(s^2 + 13s + 1.0 \cdot 10^7\right)\left(s^2 + 37s + 2.5 \cdot 10^7\right)}{\left(s^2 + 14s + 2.7 \cdot 10^6\right)\left(s^2 + 15s + 1.1 \cdot 10^7\right)\left(s^2 + 52s + 3.6 \cdot 10^7\right)}, (38)$$

$$h_{TF11} = \frac{\left(s^2 + 17s + 2.8 \cdot 10^6\right)\left(s^2 + 14s + 1.0 \cdot 10^7\right)\left(s^2 + 38s + 2.5 \cdot 10^7\right)}{\left(s^2 + 16s + 2.7 \cdot 10^6\right)\left(s^2 + 15s + 1.1 \cdot 10^7\right)\left(s^2 + 45s + 3.6 \cdot 10^7\right)}. \quad (39)$$
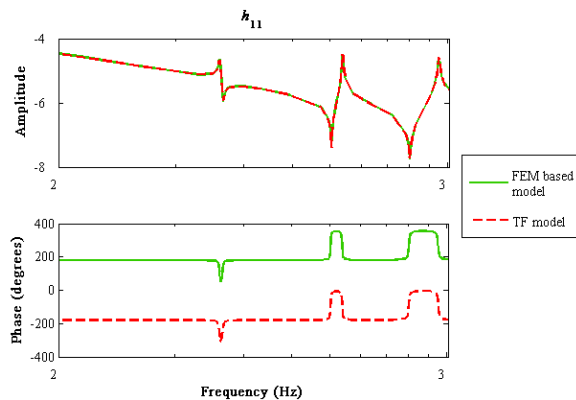
FIGURE 5: Verification of the proposed method using known FEM based model. The dashed red line is the frequency response of the calculated FEM based model and solid green line is the corresponding curve for the reconstructed FEM based model.

Figure 5 and the transfer functions (38) and (39) show that the FEM based model and the model reproduced from that using complex lead and lag compensators correspond very well with respect to both poles and zeros. Thus can be concluded that the proposed method is suitable in determining a parametric model of AMB rotor system from the FRF.

SUMMARY AND OUTLOOK

A transfer function model of flexible modes of AMB rotor system was determined first by using nonparametric identification methods for obtaining the FRF of the system, and further by utilizing complex lead and lag compensator structures to construct the transfer function matrix. The validity of the method was demonstrated comparing the frequency responses and transfer functions of the measured FRF, constructed transfer function model and FEM based model.

It was shown, that the proposed method in constructing a transfer function model gives proper results.

The identification provides effective system model that can be used to verify the original model based on FEM or EMA. System identification can also be used for fault diagnostics during operation. However, to give proper results, identification demands reliable measurement data with high signal to noise ratio. That did not realize in this examination.

In future more reliable measurement data with higher signal-to-noise ratio would be obtained. The MIMO system identification methods will be utilized to better distinguish the influence of different inputs to the outputs. Also the sine sweep signal will be replaced with stepped sine excitation.

REFERENCES

1   Lösch, F., Identification and Automated Controller Design for Active Magnetic Bearing Systems, Dissertation, ETH Zürich, Switzerland (2002).
2   Inman, D.J., Engineering Vibration, 2nd ed., 2001, Prentice Hall, United States of America, ISBN 013-0174483.
3   Gähler, C, Rotor Dynamic Testing and Control with Active Magnetic Bearings, Dissertation, ETH Zürich, Switzerland (1998).
4   Messner, W.C., Bedillion, M.D., Xia, L., Karns, D.C., Lead and Lag Compensators with Complex Poles and Zeros: Design Formulas for Modeling and Loop Shaping, IEEE Control Systems Magazine, February 2007, pp.44-54.
5   Gähler, C., Mohler, M., Herzog, R., Multivariable Identification of Active Magnetic Bearing Systems, JSME International Journal, Series C, Vol. 40, No. 4, 1997, pp. 584-592.
6   Ljung, L., System Identification, Theory for the User, 2nd edition, 1999, Prentice Hall, United States of America, ISBN 0-13-656695-2.
7   Jastrzebski, R., Design and Implementation of FPGA-Based LQ Control of Active Magnetic Bearings, Dissertation, Lappeenranta University of Technology, Finland (2007).